Research Article | Vol. 27, No. 16 | 5 Aug 2019 | OPTICS EXPRESS 22316
Optics EXPRESS

Semiconductor disk laser in bi-frequency operation by laser ablation micromachining of a laser mirror

JONATHAN WOODS,[1,*] DANIEL HEATH,[2] JAKE DAYKIN,[1] THEO CHEN SVERRE,[1] BEN KEENLYSIDE,[1] BEN MILLS,[2] ISABELLE SAGNES,[3] GREGOIRE BEAUDOIN,[3] STEPHANE BLIN,[4] ARNAUD GARNACHE,[4] ANNE TROPPER,[1] AND VASILIS APOSTOLOPOULOS[1]

[1]*School of Physics and Astronomy, University of Southampton, University Road, Southampton, Hampshire, SO17 1BJ, UK*
[2]*Optoelectronics Research Centre, University of Southampton, University Road, Southampton, Hampshire, SO17 1BJ, UK*
[3]*C2N, CNRS UMR9001, Universite Paris Sud, Palaiseau, France*
[4]*IES, CNRS UMR5214, Universite Montpellier Sud, Montpellier, France*
[*]*J.Woods@soton.ac.uk*

Abstract: We present bi-frequency continuous wave oscillation in a semiconductor disk laser through direct writing of loss-inducing patterns onto an intra-cavity high reflector mirror. The laser is a Vertical External Cavity Surface Emitting Laser which is optically pumped by up to 1.1 W of 808 nm light from a fibre coupled multi-mode diode laser, and oscillates on two Hermite-Gaussian spatial modes simultaneously, achieving wavelength separations between 0.2 nm and 5 nm around 995 nm. We use a Digital Micromirror Device (DMD) enabled laser ablation system to define spatially specific loss regions on a laser mirror by machining away the Bragg layers from the mirror surface. The ablated pattern is comprised of two orthogonal lines with the centermost region undamaged, and is positioned in the laser cavity so as to interact with the lasing mode, thereby promoting the simultaneous oscillation of the fundamental and a higher order spatial mode. We demonstrate bi-frequency oscillation over a range of mask gap sizes and pump powers.

1. Introduction

Coherent continuous wave laser sources that simultaneously oscillate on two discrete optical frequencies find applications in spectroscopy [1], radar systems, distance measurements, microwave and terahertz frequency generation [2–4] and sensing applications [5], and there exists a strong foundation of research into bi-frequency sources [6, 7]. The Vertical External Cavity Surface Emitting Laser (VECSEL) is an optically pumped semiconductor quantum well (QW) laser technology which can offer narrow emission linewidths on account of its class A dynamics and low Schawlow-Townes limit [8–11]. The combination of these factors can lead to low phase noise and good long term stability of lasing operation. Quantum well semiconductor lasers present an attractive approach to optical bi-frequency generation [9, 11–14], with the notable example of cavity spatial mode generation through innovative loss mask deposition and patterning on the VECSEL gain structure [3, 4]. The noise analysis of bi-frequency sources has been investigated in [4, 15, 16]. Bi-frequency operation has also been demonstrated through the inclusion of a birefringent filter for VECSELs [17, 18] and for a mode-locked integrated external cavity surface emitting laser (MIXSEL) [19–21] which creates two different effective cavity lengths for the two available orthogonal linear polarisation states.

We present a robust method for generating bi-frequency laser oscillation in a single laser

#365210 https://doi.org/10.1364/OE.27.022316
Journal © 2019 Received 19 Apr 2019; revised 5 Jun 2019; accepted 11 Jun 2019; published 23 Jul 2019

Optics EXPRESS

cavity using intra-cavity loss masks created by Digital Micromirror Device (DMD) enabled laser ablation machining of a dielectric Bragg mirror intrinsic to the VECSEL external cavity. The presence of spatially specific loss in the external cavity allows loss to be controlled on certain transverse cavity modes, and hence the objective is to promote oscillation of two specific spatial modes to achieve similar threshold powers, and to tune to the desired spectral separation. The technique is also remarkably fast: a simple set of cross masks may be fabricated in as little as 30 to 60 minutes.

Furthermore, because both modes share the same external cavity, and indeed because there exists a small spatial region of the gain area that is common to both spatial modes due to their partial overlap [22], noise is common to both oscillating modes and coherence may be enforced between them. Therefore, it may be possible in future to use this type of source to generate dual frequency comb emission with an inherently stable frequency beat [4]. This is a particularly important advantage because the intensity variations in highly multi-mode fibre coupled diode laser pump sources can extend well beyond 10 MHz [15, 16], which can be challenging to nullify via electronic servo stabilisation schemes. Finally, because the gain chip and the loss mask are separate, the technique presented here can be applied to any suitable laser technology without modifying a significant laser component such as the gain medium.

2. Experimental methods and fabrication

2.1. VECSEL gain design and fabrication

The VECSEL gain structure that we used was fabricated by Metallo-Organic Chemical Vapour Deposition (MOCVD) and is composed of a bottom Distributed Bragg Reflector (DBR), consisting of 31 pairs of AlAs/GaAs, followed by a $13\lambda/2$ thick microcavity gain region comprised of 6 strain-compensated InGaAs/GaAsP quantum wells, a top DBR consisting of 4 pairs of $Al_{0.18}Ga_{0.82}As$/AlAs and a GaAs capping layer. The quantum wells are positioned at field anti-nodes within the medium for a design wavelength of 1 µm, and the entire structure is resonant to provide strong spectral filtering. The gain configuration is similar to the structure that is used in [4].

2.2. Laser cavity description

The VECSEL external cavity and experimental analysis are represented schematically in Fig. 1. The cavity was formed around the VECSEL gain structure in a 24 mm long V-shape which consists of a 12.8 mm diameter, 25 mm radius of curvature concave output coupler mirror at one end of $R = 99.7\%$, and a 6 mm diameter planar high reflecting (HR) mirror ($R > 99.9\%$), onto which the masks are machined, at the other. Temperature stability of the gain structure is achieved by thermally coupling the sample to a temperature stabilised copper heat spreader. The heat spreader is maintained at 20 °C by a PID servo and thermo-electric cooler (TEC) which transfers heat into a closed-loop water cooled copper block. Respectively, the distances between the HR mirror and gain, and OC mirror and gain, are 6 mm and 18 mm. By using a V-cavity instead of a linear cavity we are able to enforce a beam waist at the mask position, thereby reducing the overall area of the ablated region, and eliminating mode astigmatism from the mask design. The choice of using a plane mirror for mask fabrication also largely eliminates issues with focusing the ablation beam onto the mirror surface, enables us to write multiple masks on one mirror and freely select which mask is interacting with the lasing mode, and allows for simple mode to mask size ratio adjustments. Up to 1.1 Watts of pump power, derived from a fibre coupled multimode laser diode, is used to optically pump the VECSEL gain structure. The fundamental and Hermite-Gaussian$_{11}$ spatial modes of the laser cavity have been calculated to have beam widths at the gain structure of 62 µm and 107 µm respectively and the fundamental Gaussian mode at the planar end mirror is 39 µm in radius. We choose a pump spot with sufficient overlap

Optics EXPRESS

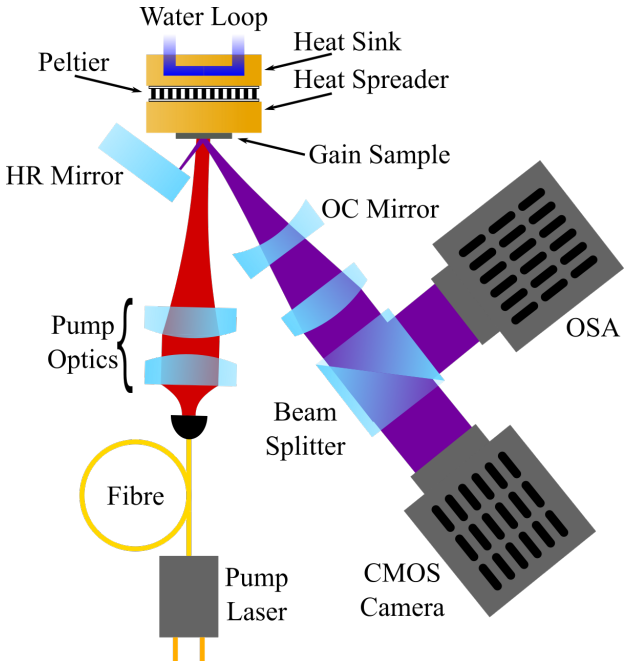

Fig. 1. Schematic diagram of the bi-frequency V-cavity VECSEL, pump configuration, with analysis equipment (CMOS camera and spectrometer). The pump laser delivers up to 1.1 W through a 60 μm core diameter fiber, which is collimated and focused onto the gain structure using 19 mm and 100 mm lenses respectively. The ablated bi-frequency masks are located on the flat HR mirror.

with the higher order spatial mode to allow for laser operation at both spatial modes. From the 60 µm core diameter (step-index) fibre, the pump light is imaged onto the gain structure with 19 mm collimation and 100 mm focusing lenses, generating a 145 µm pump spot.

2.3. *Ablated mask fabrication*

The laser machining setup used in fabricating the ablated masks, shown schematically in Fig. 2, employed a DMD (Texas Instruments DLP3000) to act as a spatial light intensity modulator. Before interaction with the DMD, 150 fs, 1 mJ pulses from a Ti:Sapphire amplifier were spatially homogenised and attenuated to the appropriate fluence. The DMD was aligned such that a spatial intensity pattern corresponding to the pattern design of ON or OFF pixels would be directed through a microscope objective onto the sample. The capabilities of this experimental setup have been explored in the works of Mills and Heath [23–26].

Loss masks were designed such that each exposure would machine a line segment 30 µm long and 1.1 µm wide when imaged at the sample. The former is within the maximum machinable area of 40 µm x 40 µm, and the latter feature width was slightly above the 952 nm resolution limit of the machining setup to avoid optical proximity effects and achieve near-uniform energy deposition.

An initial autofocus step was used to position the sample surface at the image plane of the beam line, and an image-recognition technique based on phase correlation was used to ensure correct lateral repositioning at all points of machining. In total, 8 exposures at 2.8±0.1 J/cm^2 (10% above the sample ablation threshold) were made at each position with a 50% overlap (to reduce a periodic burr pattern which often presents in laser ablation machined surfaces [27]), leading to 16 exposures in total per unit ablated area, and 512 exposures per complete mask.

Optics EXPRESS

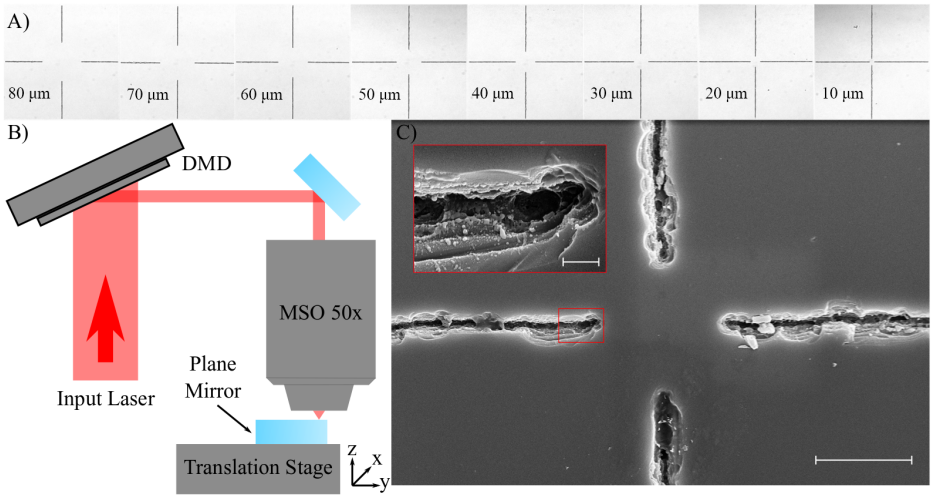

Fig. 2. Optical and electron microscope images of the ablated masks and a schematic diagram of the DMD-enabled laser ablation setup. A) A composite image showing an optical microscope image of each mask size fabricated. The distance between the outer most ends of each line is 240 µm and the distances between the innermost ends of each line (the clear aperture) range from 80 µm (left) to 10 µm (right) in divisions of 10 µm. B) 150 fs, 1 mJ optical pulses centered at 800 nm are incident on the DMD which acts as an intensity spatial light modulator. Light directed towards the microscope objective is reflected from pixels in the ON state, light reflected from the OFF state pixels is dumped. C) Scale SEM images of a 10 µm mask where the scale bar represents 10 µm (1 µm in the inset Figure).

A high number of exposures at low fluence is favoured over a small number of high fluence exposures so as to remove a small amount of material at a time, thereby limiting thermal and shock damage to surrounding regions [28].

3. Results

3.1. Dual mode operation and loss estimation

Images of the laser modes in the far field were captured with a monochrome CMOS camera as depicted in Fig. 1. The incident power was reduced by approximately 4 orders of magnitude with a reflective neutral density filter and the exposure time was set each time an image was captured to ensure that the incident intensity did not saturate the camera sensor. The first image in Fig. 3 is an example of the raw data taken by the camera. Clearly observable are modulations in the recorded intensity which, during the experiment, were determined to be the result of dust and diffraction effects occurring outside the laser cavity and not due to the ablated masks. Cleaning the raw images is achieved by a circular occlusion mask applied numerically in the frequency domain, such that only the shape of the mode field emitted from the laser remains once inverse Fourier transformed back into the spatial domain.

To determine the loss induced by the ablated masks, sample straight line masks machined onto a test mirror were analysed in a laser-based linear reflectivity setup based on the design of setup by Mangold *et al.* [29], except we use a CW Ti:Sapphire laser and the second beam chopper is omitted. The objective lens is a Mitutoyo 50x long working distance objective, achieving a waist radius of approximately 2 µm, and the line mask is translated in a direction normal to the long axis of the mask through the beam spot by piezo translation stage. For a mask fabricated with an ablation fluence of 1.8±0.1 J/cm^2 and a width of 2 µm, the reflectivity minimum was 6.2±0.1%

Optics EXPRESS

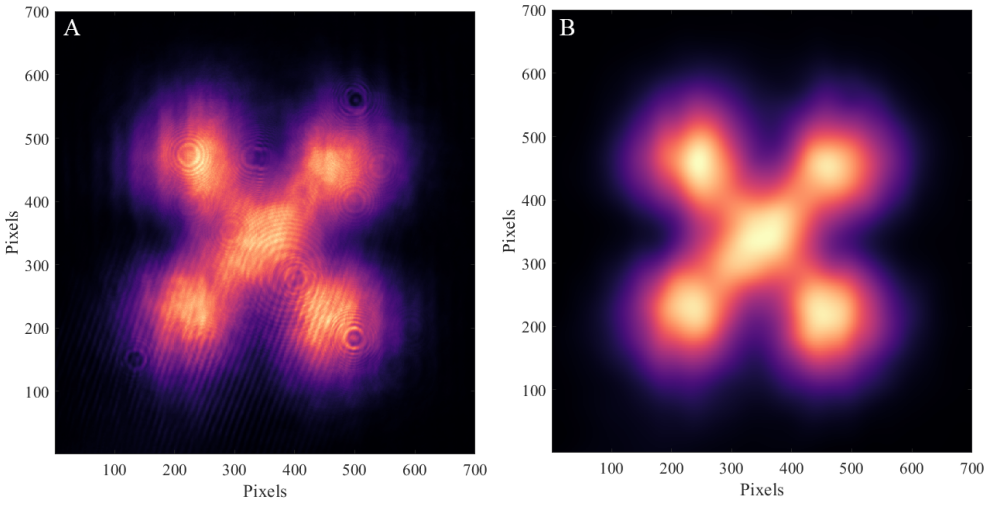

Fig. 3. Example beam profile captured by direct exposure onto a Hamamatsu ORCA Flash 4.0 CMOS camera during bi-frequency operation of the VECSEL using a 50 µm gap ablated mask. A) Raw greyscale with a linear colourmap applied in post processing. B) The same beam profile with high spatial frequency components removed through an appropriate mask in the Fourier image space. This beam profile was taken with a pump power of 1.03 W.

corresponding to a 93.8±0.1% loss. We go on to use a numerical calculation for the loss induced by the masks based on the overlap integral of a Gaussian lineshape whose magnitude in the area interacting with the mask is set to zero, and an identical unaltered Gaussian lineshape. This calculation maintains the assumption that the portion of the light incident on the ablated area is totally lost (and in the case of the laser cavity, not re-circulated in the cavity mode). For a Gaussian beam with 2 µm radius, and a line mask of width 2 µm, the calculation yields 95.3% loss.

3.2. *Clear aperture dimension analysis*

To understand how the mask clear aperture dimension influences bi-frequency lasing operation, 8 masks were fabricated with clear aperture diameters ranging from 10 µm to 80 µm in steps of 10 µm and bi-frequency lasing operation was attempted (See Fig. 4). Data for this figure is captured with an Ocean Optics HR4000 optical spectrum analyser, as per fig 1, and the pump current is altered in steps of 0.025 A. The pump power (as plotted) is derived from a pump optical power versus applied pump current calibration taken initially. It is calculated using the same technique as above, that a 40 µm mask aperture would provide 0.6% loss to the 39 µm radius fundamental mode and negligible loss to the HG_{11}, which, coupled with the higher pump intensity for the fundamental would approximately equalise the threshold pump powers for both modes.

In the case of the 10 and 20 µm aperture masks, stable bi-frequency oscillation was not achieved. Emission of only the HG_{11} mode is observed because the overlap of the HG_{00} spatial mode with the mask introduces sufficient loss to prohibit lasing at all available pump powers - calculated to be 9.4% and 4.7% loss respectively. The rate of spectral tuning of the HG_{11} modes for both masks is predominantly the result of thermal tuning within the pump spot [3,4].

An important feature of the data in Fig. 4 is the switching of the lasing onset order of the two spatial modes between the 30 and 40 µm masks. For a 40 µm fundamental beam radius, the mask clear aperture radius which satisfies the condition for equal modal intra-cavity round trip losses for the two modes (and hence equal threshold pump powers) lies between 30 and 40 µm aperture. These two mask sizes provide 1.9% and 0.6% loss respectively for the fundamental

Optics EXPRESS

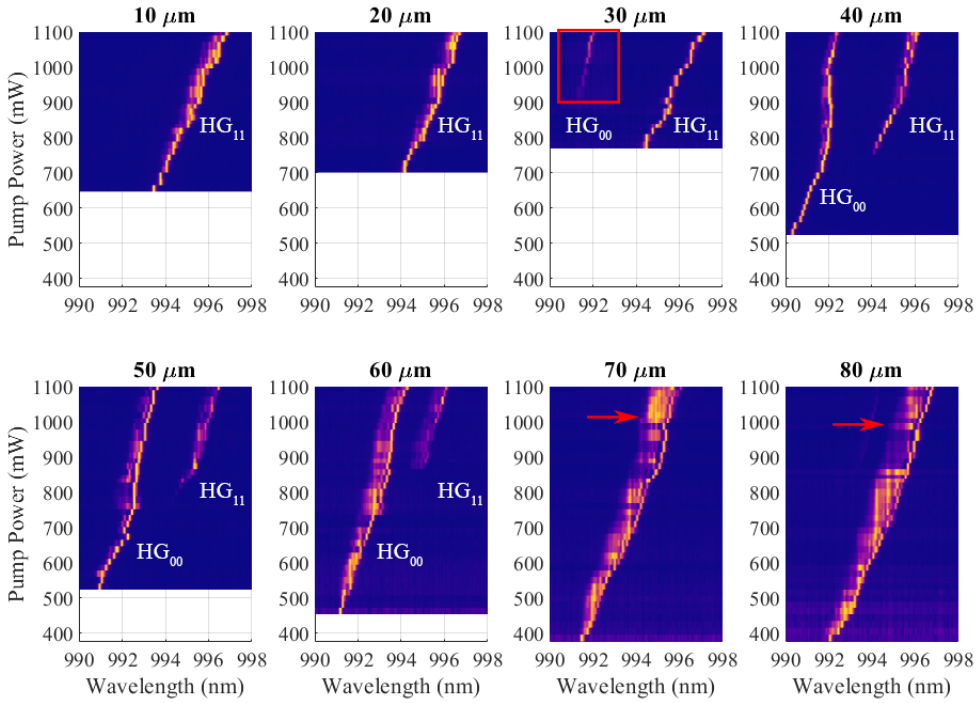

Fig. 4. The maximum amplitude of each spectrum is normalised to unity on a linear scale, and the baseline amplitude of each spectrum is reduced to zero by dark count subtraction after 20 minutes of run time for the spectrum analyser. The magnitude for the spectral data in the red boxed area 30 μm mask around the HG_{00} mode has been increased by a factor of 5 for visibility. The masks were fabricated with an ablation power of 2.8±0.1 J/cm^2, on a 99.98% dielectric mirror from Layertec GmbH (6 mm diameter, 3 mm substrate thickness, coating number 114096). Respectively, the maximum output powers for each mask was 9.61, 9.00, 2.28, 7.67, 9.79, 11.73, 13.47 and 15.70 mW, and the pump power at maximum current was 1.1 W with a slope efficiency of 0.73W/A. For the 70 and 80 μm masks the two spatial modes overlap spectrally, therefore the red arrow in each plot shows at what pump power the HG_{11} mode reaches threshold.

mode. A further important feature is that where the mask provides strong spatial overlap with the HG_{00} mode at 30 and 40 μm aperture diameter, the loss per round trip is sufficient to maintain a narrow linewidth. At a mask aperture of 50 μm and above, the mask-induced loss is decreased and broadening in the spatial mode linewidth is observed. It is possible to counterbalance this by increasing the net output coupling of the cavity, or shortening the cavity length to decrease the cavity lifetime for less spatially aggressive masks.

Onset of the HG_{11} mode in the 40-60 micron masks appears to coincide with an alteration in the behaviour of the wavelength tuning with respect to pump power of the fundamental modes. The rate of red tuning with linearly increasing pump power slows for the 50 and 60 micron masks and even halts for the 40 micron mask when the threshold for the respective HG_{11} mode is reached. For the 70 and 80 μm masks, no spectral shift due to the onset of the HG_{11} mode is observed and the two spatial modes are not separated in frequency despite visibility of the two spatial modes on the beam camera towards the upper limit of available pump power. We note that the wavelength at threshold for the fundamental mode does not change significantly between the different masks, only the pump power at which threshold occurs.

The gain sample we employ in this work has a small signal gain of approximately 5 - 10%,

Optics EXPRESS

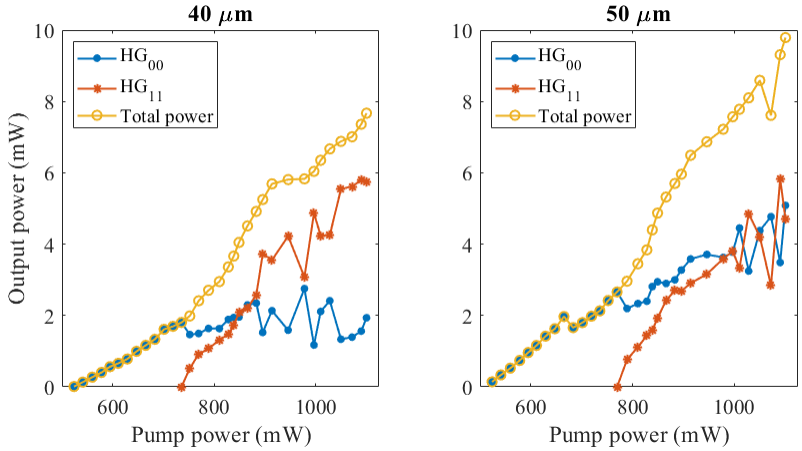

Fig. 5. Power per spatial mode as a function of incident pump power for the 40 µm and 50 µm aperture size loss masks. Relative modal power values were computed from (non-saturated) beam profile images taken using a CMOS camera in conjunction with the total measured beam power.

while the total losses (excluding the mask induced losses) are assumed to be approximately 1%. Therefore beyond lasing threshold, by increasing the mask clear aperture for a given pump power, or indeed by increasing the pump power for a given mask, the total cavity losses fall below that of the maximum available gain and the laser is able to oscillate on multiple axial modes. This has the effect of increasing the apparent linewidth of the emission.

From an application perspective, the modulation depth of the beat frequency between the two spatial modes is of specific importance. As such, it is crucial that the relative powers per mode are comparable to each other. Plotted in Fig 5 is the computed power per mode for the 40 µm and 50 µm masks corresponding to the spectral data in Fig 4. The power values are obtained by processing the beam profile images similar to Fig 3 which were taken at each pump power. The calculation is performed by finding the ratio of the integral of the smoothed original beam profile to the integral of the smoothed beam profile with a numerically fitted fundamental spatial mode subtracted from it (leaving just the HG_{11}), and normalising to the measured total beam power. The monochrome raw images are captured at 16 bit depth, the stated sensor linearity is $< 3\%$, and the camera exposure is altered on a per still exposure basis to avoid saturation.

Following onset of the HG_{11} mode in the 40 µm through 60 µm masks, it is observed that with increasing pump power the wavelength separation of the two spatial modes is also increasing; this is associated with a change in the rate of tuning of the fundamental mode. If we take the peak wavelength separation values for the 30 and 40 µm masks and convert them to frequency, we show a tuning range of 0.23 THz between beat notes of 1.32 THz (at 946 mW) and 1.55 THz (at 1100 mW) for the 30 µm mask, and 0.42 THz between beat notes of 0.68 THz (at 752 mW) and 1.10 THz (at 978 mW) for the 40 µm mask; which correspond to 1.48 THz/W and 1.89 THz/W, respectively.

3.3. *Temporal stability*

While the laser ablation setup was being calibrated and tested, we fabricated a series of masks that, although successful in generating bi-frequency emission, contained significant errors in fabrication. In these masks the geometrical center of the circle defined by the perimeter of each mask clear aperture did not reside at the crossing point of the orthogonal lines which form the masks - one was typically offset from the other by up to 26% of the mask aperture diameter.

Optics EXPRESS

Bi-frequency spectral results for these initial results are presented in reference [30]. These masks introduced more loss both to the HG_{00} and HG_{11} modes, which is evident also because these modes had 50% higher threshold than the results presented in Fig. 6. These masks demonstrated what we believe was single longitudinal mode operation in both spatial modes, on account of the increased spatial loss. Increasing the cavity loss increases the gain, which enhances the gain spectral filtering, creating the conditions for single longitudinal mode operation.

Bi-frequency operation was tested with a cavity identical to the schematic in fig. 1, except the 25mm curved mirror is now a high reflector, and plane mirror (on which the masks were fabricated) is a 0.3% transmission partial reflector, so as to maintain a consistent level of cavity output coupling. Plotted in Fig. 6A is the operating wavelength as a function of pump current. We note that for regions consisting of multiple pump current steps, the emission wavelength does not appear to change. It is noticeable however that as the pump current increases the relative power per mode shifts in favour of higher power in the longer wavelength mode before a spectral shift occurs in both modes: this is particularly apparent between 1.4 A and 1.65 A. The noted trend supports the notion that the gain spectral peak is red shifting with increasing current as expected for this type of laser. The otherwise stepwise appearance is due to the 0.025A step size change in pump current.

Plotted in Fig. 6B top is a timelapse of 100 sequential optical spectra (Yokogawa AQ6370D) taken for the laser oscillating in bi-frequency operation over a period of approximately 80 seconds, taken at a spectral resolution of 0.02 nm. This data was processed to find the spectral peak wavelengths for each component within each spectrum, and the wavelength difference is plotted in the Fig. 6B bottom. The variation in the difference values does not exceed the resolution limit of the measurements, suggesting that each component is a single longitudinal mode, as the free spectral range (6.24 GHz) of the external cavity is approximately the same as the resolution limit of the OSA.

We further tested the purity of operation by spatially selecting and coupling to a multimode

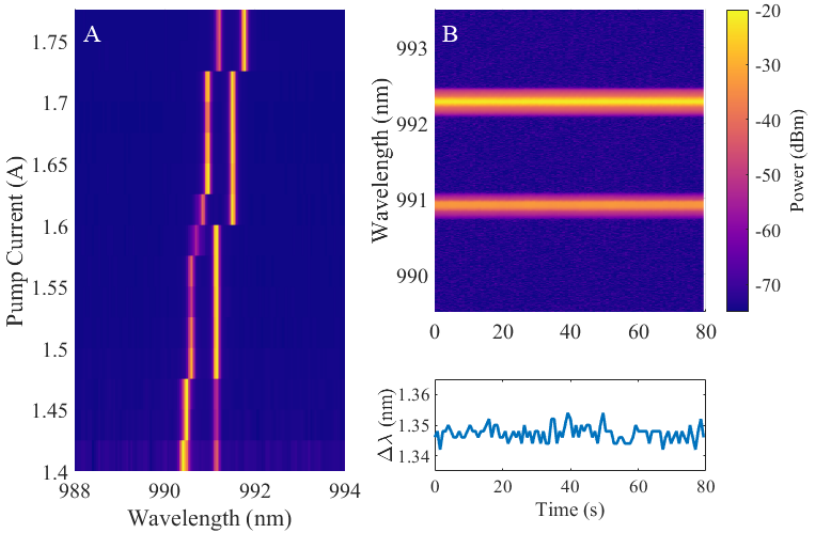

Fig. 6. Bi-frequency spectral tuning and temporal evolution data over a period of nearly 80 seconds. A) Bi-frequency operation as a function of pump current. B top) 100 spectra were captured with a time between acquisitions of 0.79 seconds, and all with a machine-limited spectral resolution of 0.02 nm (6.12 GHz). B bottom) Wavelength difference between the peak power for each spatial mode. The mean spectral separation is 1.347 nm (411.1 GHz).

Optics EXPRESS

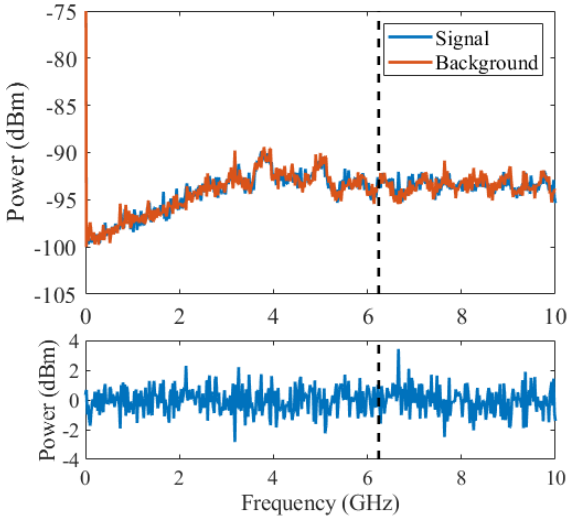

Fig. 7. Top) Signal and background RF traces for the VECSEL operating in bi-frequency. The background trace represents the same configuration with only the beam blocked at the fiber launcher, and the VBW and RBW are 10 kHz for both traces. Bottom) Shows the residual between the two top traces. The black line highlights the cavity Free Spectral Range frequency of 6.24 GHz.

fibre a region shared by both spatial modes and directed this onto a 25 GHz bandwidth, multimode fiber coupled input, fast photodiode connected to a RF spectrum analyser of similar bandwidth. See Fig. 7. The RF spectrum is clean, with no evidence of adjacent longitudinal mode beating. As part of future work, confirming single longitudinal mode operation may be achieved through beating of the laser operating in bi-frequency against a stable frequency comb and observing the RF spectrum.

4. Conclusion

We have shown a method for generating bi-frequency laser oscillation in a single laser cavity using intra-cavity loss masks created by laser ablation machining of a dielectric Bragg mirror intrinsic to the external cavity of a VECSEL. Our results shown that the threshold of the HG modes can be tailored with the dimensions of the mask and our technique is both robust against fabrication errors and easy to implement. Furthermore, the gain chip and the loss mask are separate, therefore the technique presented here can be applied to any suitable laser technology in a way that does not modify a crucial element of the laser such as the gain medium. Because the two modes have a shared region of the gain, noise is common to both oscillating modes and coherence may be enforced between them, which is partly what is suggested by our measurement of temporal stability of the spectra of the two lasing modes. In future work we will explore the possibility of using this technique in order to achieve bi-frequency operation in mode-locked lasers which can lead to a dual frequency comb spectrometer.

All data supporting this study are openly available from the University of Southampton repository at: https://doi.org/10.5258/SOTON/D0874

Funding

Engineering and Physical Sciences Research Council (EPSRC) (EP/M013294/1, EP/N03368X/1).

Optics EXPRESS

References

1. P. Dumont, F. Camargo, J. Danet, D. Holleville, S. Guerandel, G. Pillet, G. Baili, L. Morvan, D. Dolfi, I. Gozhyk, G. Beaudoin, I. Sagnes, P. Georges, and G. Lucas-Leclin, "Low-noise dual-frequency laser for compact cs atomic clocks," J. Light. Technol. **32**, 3817–3823 (2014).
2. G. Danion, C. Hamel, L. Frein, F. Bondu, G. Loas, and M. Alouini, "Dual frequency laser with two continuously and widely tunable frequencies for optical referencing of ghz to thz beatnotes," Opt. Express **22**, 17673–17678 (2014).
3. R. Paquet, S. Blin, M. Myara, L. L. Gratiet, M. Sellahi, B. Chomet, G. Beaudoin, I. Sagnes, and A. Garnache, "Coherent continuous-wave dual-frequency high-q external-cavity semiconductor laser for ghz–thz applications," Opt. Lett. **41**, 3751–3754 (2016).
4. S. Blin, R. Paquet, M. Myara, B. Chomet, L. L. Gratiet, M. Sellahi, G. Beaudoin, I. Sagnes, G. Ducournau, P. Latzel, J. Lampin, and A. Garnache, "Coherent and tunable thz emission driven by an integrated iii-v semiconductor laser," IEEE J. Sel. Top. Quantum Electron. **23**, 1–11 (2017).
5. L. Chaccour, G. Aubin, K. Merghem, J. Oudar, A. Khadour, P. Chatellier, and S. Bouchoule, "Cross-polarized dual-frequency vecsel at 1.5 µm for fiber-based sensing applications," IEEE Photonics J. **8**, 1–10 (2016).
6. L. Xiao, S. Trebaol, Y. Dumeige, Z. Cai, M. Mortier, and P. Feron, "Miniaturized optical microwave source using a dual-wavelength whispering gallery mode laser," IEEE Photonics Technol. Lett. **22**, 559–561 (2010).
7. G. Ducournau, P. Szriftgiser, T. Akalin, A. Beck, D. Bacquet, E. Peytavit, and J. F. Lampin, "Highly coherent terahertz wave generation with a dual-frequency brillouin fiber laser and a 1.55 µm photomixer," Opt. Lett. **36**, 2044–2046 (2011).
8. G. Baili, F. Bretenaker, M. Alouini, L. Morvan, D. Dolfi, and I. Sagnes, "Experimental investigation and analytical modeling of excess intensity noise in semiconductor class-a lasers," J. Light. Technol. **26**, 952–961 (2008).
9. G. Baili, L. Morvan, M. Alouini, D. Dolfi, F. Bretenaker, I. Sagnes, and A. Garnache, "Experimental demonstration of a tunable dual-frequency semiconductor laser free of relaxation oscillations," Opt. Lett. **34**, 3421–3423 (2009).
10. A. Laurain, M. Myara, G. Beaudoin, I. Sagnes, and A. Garnache, "Multiwatt—power highly—coherent compact single—frequency tunable vertical—external—cavity—surface—emitting—semiconductor—laser," Opt. Express **18**, 14627–14636 (2010).
11. S. De, G. Baili, M. Alouini, J.-C. Harmand, S. Bouchoule, and F. Bretenaker, "Class-a dual-frequency vecsel at telecom wavelength," Opt. Lett. **39**, 5586–5589 (2014).
12. V. Pal, P. Trofimoff, B.-X. Miranda, G. Baili, M. Alouini, L. Morvan, D. Dolfi, F. Goldfarb, I. Sagnes, R. Ghosh, and F. Bretenaker, "Measurement of the coupling constant in a two-frequency vecsel," Opt. Express **18**, 5008–5014 (2010).
13. A. Chernikov, M. Wichmann, M. K. Shakfa, M. Scheller, J. V. Moloney, S. W. Koch, and M. Koch, "Time-dynamics of the two-color emission from vertical-external-cavity surface-emitting lasers," Appl. Phys. Lett. **100**, 041114 (2012).
14. M. Scheller, C. W. Baker, S. W. Koch, J. V. Moloney, and R. J. Jones, "High power dual-wavelength vecsel based on a multiple folded cavity," IEEE Photonics Technol. Lett. **29**, 790–793 (2017).
15. S. De, A. E. Amili, I. Fsaifes, G. Pillet, G. Baili, F. Goldfarb, M. Alouini, I. Sagnes, and F. Bretenaker, "Phase noise of the radio frequency (rf) beatnote generated by a dual-frequency vecsel," J. Light. Technol. **32**, 1307–1316 (2014).
16. S. De, A. E. Amili, G. Pillet, G. Baili, F. Goldfarb, M. Alouini, I. Sagnes, and F. Bretenaker, "Experimental and theoretical study of noise in a dual-frequency vecsel," Proc.SPIE **8966**, 8966 – 8966 – 14 (2014).
17. H. Liu, G. Gredat, G. Baili, F. Gutty, F. Goldfarb, I. Sagnes, and F. Bretenaker, "Noise investigation of a dual-frequency vecsel for application to cesium clocks," J. Light. Technol. **36**, 3882–3891 (2018).
18. G. Gredat, D. Chatterjee, G. Baili, F. Gutty, I. Sagnes, F. Goldfarb, F. Bretenaker, and H. Liu, "Fully correlated multimode pumping for low noise dual frequency vecsels," Opt. Express **26**, 26217–26226 (2018).
19. S. M. Link, D. J. H. C. Maas, D. Waldburger, and U. Keller, "Dual-comb spectroscopy of water vapor with a free-running semiconductor disk laser." Science **356**, eaam7424–10 (2017).
20. S. M. Link, A. Klenner, and U. Keller, "Dual-comb modelocked lasers: semiconductor saturable absorber mirror decouples noise stabilization," Opt. Express **24**, 1889–1902 (2016).
21. S. M. Link, A. Klenner, M. Mangold, C. A. Zaugg, M. Golling, B. W. Tilma, and U. Keller, "Dual-comb modelocked laser," Opt. Express **23**, 5521–5531 (2015).
22. R. Paquet, S. Blin, M. Myara, L. Le Gratiet, M. Sellahi, B. Chomet, G. Beaudoin, I. Sagnes, and A. Garnache, "Coherent continuous-wave dual-frequency high-Q external-cavity semiconductor laser for GHz-THz applications," Opt. Lett. **41**, 3751–3754 (2016).
23. B. Mills, D. J. Heath, M. Feinaeugle, J. A. Grant-Jacob, and R. W. Eason, "Laser ablation via programmable image projection for submicron dimension machining in diamond," J. Laser Appl. **26**, 041501 (2014).
24. D. J. Heath, B. Mills, M. Feinaeugle, and R. W. Eason, "Rapid bespoke laser ablation of variable period grating structures using a digital micromirror device for multi-colored surface images," Appl. Opt. **54**, 4984–4988 (2015).
25. D. J. Heath, J. A. Grant-Jacob, M. Feinaeugle, B. Mills, and R. W. Eason, "Sub-diffraction limit laser ablation via multiple exposures using a digital micromirror device," Appl. Opt. **56**, 6398–6404 (2017).
26. D. J. Heath, J. A. Grant-Jacob, R. W. Eason, and B. Mills, "Single-pulse ablation of multi-depth structures via spatially filtered binary intensity masks," Appl. Opt. **57**, 1904–1909 (2018).
27. R. Geremia, D. Karnakis, and D. P. Hand, "The role of laser pulse overlap in ultrafast thin film structuring applications," Appl. Phys. A **124** (2018).

Optics EXPRESS

28. E. G. Gamaly, A. V. Rode, B. Luther-Davies, and V. T. Tikhonchuk, "Ablation of solids by femtosecond lasers: Ablation mechanism and ablation thresholds for metals and dielectrics," Phys. Plasmas **9**, 949–957 (2002).
29. M. Mangold, V. J. Wittwer, O. D. Sieber, M. Hoffmann, I. L. Krestnikov, D. A. Livshits, M. Golling, T. SÃijdmeyer, and U. Keller, "Vecsel gain characterisation," Opt. Express **20**, 4136 (2012).
30. J. Woods, D. Heath, J. Daykin, T. C. Sverre, B. Mills, A. Garnache, A. Tropper, and V. Apostolopoulos, "Towards dual frequency comb vecsels with dmd laser-ablated spatial mode masks," Proc. SPIE **10901** (2019).